Comparison of multiple reanalysis datasets with gridded precipitation observations over the Tibetan Plateau

Qinglong You [1]*, Jinzhong Min[1], Wei Zhang[1], Nick Pepin[2], Shichang Kang[3]

1. Earth System Modelling Center (ESMC), Nanjing International Academy of Meteorological Sciences (NIAMS); Key Laboratory of Meteorological Disaster, Ministry of Education; Collaborative Innovation Center on Forecast and Evaluation of Meteorological Disasters; Nanjing University of Information Science and Technology, Nanjing, 210044, China;
2. Department of Geography, University of Portsmouth, U.K. ;
3. State Key Laboratory of Cryospheric Science, Chinese Academy of Sciences, Lanzhou 730000, China;

* Corresponding author E-mail address: yqingl@126.com

Resubmitted to *Climate Dynamics*, July 22, 2014

Abstracts: Precipitation is a critical component of the water balance, and hence its variability is critical for cryospheric and climate change in the Tibetan Plateau (TP). Mean annual and seasonal precipitation totals are compared between gridded observations interpolated to a high resolution (0.25°×0.25°) and multiple reanalysis type-datasets during 1979-2001. The latter include two NCEP reanalyses (NCEP1 and NCEP2), two European Centre for Medium-Range Weather Forecasts (ECMWF) reanalyses (ERA-40 and ERA-Interim), three modern reanalyses (the 20th century reanalysis (20century), MERRA and CFSR) and three merged analysis datasets (CMAP1, CMAP2 and GPCP). Observations show an increase in mean precipitation from the northwestern (NW) to the southeastern (SE) regions of the TP which are divided by an isohyet of 400 mm, and overall trends during the studied period are positive. Compared with observations, most of the datasets (NCEP1, NCEP2, CMAP1, CMAP2, ERA-Interim, ERA-40, GPCP, 20century, MERRA and CFSR) can both broadly capture the spatial distributions and identify temporal patterns and variabilities of mean precipitation. However, most multi-datasets overestimate precipitation especially in the SE where summer convection is dominant. There remain substantial disagreements and large discrepancies in precipitation trends due to differences in assimilation systems between datasets. Taylor diagrams are used to show the correlation coefficients, standard deviation, and root-mean-square difference (RMSD) of precipitation totals between interpolated observations and assimilated values on an annual and seasonal basis. Merged analysis data (CMAP1, CMAP2 and GPCP) agree with observations more closely than reanalyses. Thus not all datasets are equally biased and choice of dataset is important.

Key words: Precipitation; multi-datasets, observation; Tibetan Plateau

1. Introduction

According to the Intergovernmental Panel on Climate Change (IPCC) Fifth Assessment Report (AR5), global mean surface temperatures have warmed by 0.85 (+/-0.2) ℃ between 1880 and 2012 [*IPCC*, 2013]. The Clausius-Clapeyron equation shows that the water holding capacity of air increases by about 7% per degree of warming, leading to increased water vapor in the atmosphere [*Trenberth*, 2011]. Thus warming could change the amount, intensity, frequency, type, extremes and patterns of precipitation, accelerating the hydrological cycle and increasing extreme events (such as floods and droughts) [*Ohmura and Wild*, 2002; *Trenberth*, 2011]. While extreme precipitation events may become more common in a warmer climate, many predictions of future changes in precipitation extremes may be underestimated [*Allan and Soden*, 2008]. In recent decades, changes in precipitation have attracted much attention. Precipitation is not only a major component of the global hydrological cycle, but also influences the development of all living organisms [*IPCC*, 2007; *Joshi and Pandey*, 2011; *Trenberth*, 2011; *Trenberth and Guillemot*, 1998]. Much societal infrastructure and property is becoming more sensitive to precipitation extremes, making the causes and predictability of precipitation variability of great importance.

The Tibetan Plateau (TP) with an average elevation of over 4000 m a.s.l., is called “the roof of the world”, and influences global atmospheric circulation through both thermal and mechanical forcing [*Duan and Wu*, 2005; *Yeh and Gao*, 1979]. The TP is also the source of many rivers in South and East Asia, such as the Indus, Ganges-Brahmaputra, Yangtze, and is called “the world water tower” [*X D Xu et al.*, 2008]. It is one of the most active centers of the hydrological cycle in the world [*Feng and Zhou*, 2012]. In recent decades, both climate and the cryosphere in the TP are undergoing rapid change [*Kang et al.*, 2010; *Qiu*, 2008], which will have profound effects on the

Asian "water towers" [*Immerzeel et al.*, 2010]. However, due to limited availability of accurate observations, especially in the western TP, there are limited studies focusing on hydrological responses to climate change and the mechanisms are seldom discussed [*Yang et al.*, 2011].

Precipitation in the TP varies both in space and time, and has significantly increased during recent decades in certain areas based on adjusted station data [*You et al.*, 2012]. Many studies have examined precipitation trends in the TP and demonstrate the link between precipitation and atmospheric/oceanic circulation indices, including the North Atlantic Oscillation (NAO), ENSO, the Indian Ocean Dipole, the Asian-Pacific Oscillation, and the Asian monsoon [*Duan et al.*, 2012; *Joshi and Pandey*, 2011; *Liu and Yin*, 2001]. However, different researchers calculate correlations using different gridded precipitation datasets, which leads to remarkable inconsistency among results. In addition, observations are particularly scarce in many regions because of rigorous environmental conditions (such as desert). Thus understanding of the current and future precipitation variability depends in part on rigorous evaluation of the many contrasting "datasets" in the region, often a difficult task. Datasets include reanalyses, satellite products, gauge observations, and mixtures of different data sources, often interpolated to a regular grid. Gridded "observations" have been widely used by climate community, because of their spatial and temporal continuity. Regular reanalyses include: The National Centers for Environmental Prediction/National Center for Atmospheric Research Reanalysis (NCEP/NCAR hereafter) [*Kalnay et al.*, 1996; *Kistler et al.*, 2001]; The European Centre for Medium-Range Weather Forecasts (ECMWF) 40 years reanalysis (ERA-40 hereafter) [*Uppala et al.*, 2005]; and the new ECMWF reanalysis ERA-Interim [*Dee et al.*, 2011]. NCEP/NCAR has two versions: NCEP/NCAR 1 reanalysis (NCEP1 hereafter) [*Kalnay et al.*, 1996] and NCEP/NCAR 2

89 reanalysis (NCEP2 hereafter) [*Kistler et al.*, 2001]. Both NCEP1 and NCEP2 share similar input
90 raw data and vertical and horizontal resolution (T62, 28 levels, 6 hours), while NCEP2 is an
91 updated and human error-fixed version of NCEP1 [*Kanamitsu et al.*, 2002]. Modern reanalyses
92 include the 20th century reanalysis (20century hereafter) [*Compo et al.*, 2011], the Modern-Era
93 Retrospective Analysis for Research and Application (MERRA hereafter) [*Rienecker et al.*, 2011]
94 and the NCEP Climate Forest System Reanalysis (CFSR hereafter) [*Saha et al.*, 2010].
95 Precipitation estimates are also provided from merged satellite and gauge observations (gridded).
96 The NOAA Climate Prediction Center (CPC) Merged Analysis of Precipitation (CMAP hereafter)
97 is widely used, which produces monthly analyses of global precipitation in which gauge
98 observations are merged with precipitation estimates from several satellite-based algorithms
99 (infrared and microwave) [*Xie and Arkin*, 1997]. CMAP contains two versions: standard CMAP
100 (CMAP1 hereafter) and enhanced CMAP (CMAP2 hereafter) [*Xie and Arkin*, 1997]. Compared
101 with CMAP1, CMAP2 includes not only the satellite estimates, but also blended NCEP/NCAR
102 reanalysis precipitation values. The Global Precipitation Climatology Project (GPCP) Version
103 2.1 monthly precipitation dataset (GPCP hereafter) also combines gauge observations and
104 satellite precipitation data [*Adler et al.*, 2003; *Huffman et al.*, 1997]. However it is produced
105 using different techniques and types of input data [Yin et al., 2004].
106 The objective of this study is to compare multiple datasets of precipitation (NCEP1, NCEP2,
107 CMAP1, CMAP2, ERA-Interim, ERA-40, GPCP, 20century, MERRA and CFSR) with available
108 gridded observations over the TP. Similarities and differences in precipitation on an annual and
109 seasonal basis (summer: DJF; autumn: MAM; winter: JJA; spring: SON) are investigated.
110

2. Data and Methods

2.1 Observations and multi-datasets

Precipitation observations are derived from a new monthly gridded dataset at 0.25° resolution, provided by the National Climate Center of China Meteorological Administration (NCC/CMA). Interpolation is based on an "anomaly approach" using over 2400 stations [*Wu and Gao*, 2013; *Xu et al.*, 2009], which is similar to the method used to create the CRU (Climatic Research Unit) dataset [*New et al.*, 2002]. This consists of two steps [*New et al.*, 2002; *Wu and Gao*, 2013; *Xu et al.*, 2009]. Firstly, a 30-year mean daily temperature for 1971–2000 is calculated for each Julian date at each station. Then, the mean is interpolated to a regular 0.25° × 0.25° grid. In the second step, a daily deviation for 1961–2005 is created relative to the 1971–2000 reference period for each contributing station. The deviations are then gridded as anomalies. Finally, the high resolution-gridded observation for the full 1961-2005 period is derived by adding the anomalies to the climatology. This dataset has been widely used to validate regional and global atmospheric model simulations of extreme precipitation indices. Compared with station density over eastern China, there are few stations over western China, where the density of population and urban establishments is much lower. In particular no stations are found over the northwestern part of the Tibetan Plateau, a region largely uninhabited [*Xu et al.*, 2009]. Thus, the TP can be divided into northwestern (NW) and southeastern (SE) regions using the mean annual isohyet of 400 mm (Figure 1 top left).

Monthly mean precipitation rates from NCEP1 and NCEP2 reanalyses are provided by NOAA/OAR/ESRL PSD, Boulder, Colorado, USA. The short-term precipitation rate is converted to monthly amount NCEP1 and NCEP2 start from January 1948 and January 1979 respectively,

and both have a spatial resolution of 2.5°×2.5° [*Kalnay et al.*, 1996; *Kistler et al.*, 2001]. Monthly mean precipitation rates (mm/day) were converted to mm/month. Both NCEP1 and NCEP2 precipitation reanalyses use intermittent data assimilation based on a T62 model with 28 vertical sigma levels and the Operational Statistical Interpolation (SSI) procedure [*Serreze and Hurst*, 2000]. Convective and large-scale precipitation are computed separately. The convection scheme has been shown to improve precipitation simulations over the Continental United States and in the tropics, and the large-scale precipitation is parameterized using a top-down approach with checking for super-saturation [*Kalnay et al.*, 1996]. Both NCEP1 and NCEP2 have produced realistic precipitation in high latitudes over both Asia and North America [*Kistler et al.*, 2001]. They have the same spatial and temporal resolution, but NCEP2 (after 1979) uses an improved assimilation procedure based on 4D-variational assimilation. Additional errors in NCEP1 including the issue of Southern Hemisphere bogus data (1979-1992) and errors in snow cover (1974-1994) have been fixed in NCEP2 [*Kanamitsu et al.*, 2002].

CMAP contains a collection of precipitation datasets with a spatial resolution of 2.5°×2.5°, constructed from gauge data and satellite-derived estimates [*Xie and Arkin*, 1997]. CMAP1 merges gauge observations and satellite estimates without NCEP/NCAR reanalysis, but CMAP2 also includes a reanalysis component [*Xie and Arkin*, 1997]. Gauge observations contain precipitation distributions with full global coverage and improved quality. Satellite estimates are obtained through combining the Geostationary Operational Environmental Satellite (GOES) Precipitation Index (GPI); an outgoing longwave radiation (OLR)-based Precipitation Index (OPI); a Special Sensor Microwave/Imager (SSM/I) scattering index; and Microwave Sounding Unit (MSU) [*Xie and Arkin*, 1997]. Therefore both CMAP1 and CMAP2 are dependent on the amount

155 of gauge data and the accuracy of satellite estimates (best in the tropics and weakest in the polar
156 regions). However past study has demonstrated their use in climate analysis, numerical model
157 validation and hydrological research [*Xie and Arkin*, 1997].

158 The monthly mean surface precipitation in ERA-40 reanalysis is obtained from ECMWF,
159 available from September 1957 to August 2002 with a spatial resolution of 2.5°×2.5° [*Uppala, et*
160 *al.*, 2005]. This is based on a fixed intermittent data assimilation scheme. The forecast model has a
161 horizontal resolution of T106 with 31 vertical levels and uses three-dimensional semi-Lagrangian
162 advection. An intermittent statistical optimal interpolation is used in ERA-40 precipitation output
163 which requires model initialization [*Serreze and Hurst*, 2000]. ERA-40 calculates liquid
164 precipitation and snowfall separately, and convective and large-scale precipitation are added to
165 produce total precipitation [*Ma et al.*, 2009].

166 The newer ECMWF reanalysis ERA-Interim [*Dee et al.*, 2011] has improved correction of
167 satellite observations and the more recent ECMWF model is used for the period since 1979 with a
168 spatial resolution of 1.5°×1.5°. Many have concluded that ERA-Interim yields much more realistic
169 results, with significant improvements in the global hydrological cycle [*Betts et al.*, 2009].

170 GPCP is the result of an international project of the WMO/WCRP/GEWEX designed to
171 provide improved long-record estimates of precipitation over the globe. The monthly dataset at
172 2.5° resolution from 1979 to present incorporates estimates from low-orbit satellite microwave
173 data, geosynchronous-orbit satellite infrared data, and surface rain gauge observations [*Adler et al.*,
174 2003; *Huffman et al.*, 1997]. The final merged product incorporates the advantages of each data
175 type, and removes bias in a stepwise approach. GPCP has been applied to validate climate models,

model-based reanalyses, calibrate hydrological models, and has been compared with experimental precipitation estimation techniques [*Adler et al.*, 2003; *Huffman et al.*, 1997].

Reanalysis of 20century is based on objectively-analyzed four-dimensional weather maps from 1871-2011, including uncertainty estimates. An ensemble filter is used to assimilate surface pressure reports and uses observed monthly sea-surface temperature and sea-ice distributions as boundary conditions [*Compo et al.*, 2011]. It is also a valuable resource to the climate research community for both model validation and diagnostic studies.

MERRA has been produced by NASA's Global Modeling and Assimilation Office with two primary objectives: (1) to place observations from NASA's Earth Observing System satellites into a climate context and (2) to improve hydrological cycle representations in earlier generations of reanalyses [*Rienecker et al.*, 2011]. Focusing on the satellite era from 1979 to the present, MERRA claims significant improvements in precipitation and water vapor climatology compared with older reanalyses, providing vertical integrals and analysis of increment fields for the closure of atmospheric budgets [*Rienecker et al.*, 2011].

Finally, CFSR produced at NCEP covers the period from 1979 to the present, which is considerably more accurate than the previous global reanalysis made at NCEP [*Saha et al.*, 2010]. Meanwhile, it is more comprehensive because it includes analyses of both the ocean and sea ice, and has higher resolution in space and time [*Saha et al.*, 2010]. Similar to ERA-Interim, these latest reanalysis systems (20century, MERRA and CFSR) are more advanced than the earlier versions. Meanwhile, these reanalyses provide higher spatial resolution and yield more detailed climate features at small scales [*Zhang et al.*, 2013].

197 All of these 10 datasets are compared with the observational dataset over the TP region. The
198 domain covers the area from 25°N-40°N and 86°E-105°E. Table 1 provides a summary of critical
199 features of each dataset. A comparable period of 1979-2001 is selected for all analyses.

200 **2.2 Methods**

201 To quantify similarities and differences between the observations and the other datasets, a
202 Taylor diagram [*Taylor*, 2001] is employed to facilitate comparisons. This provides a concise
203 statistical summary of how well each dataset matches the observations in terms of their correlation
204 coefficient (R), their root-mean-square difference (RMSD), and the ratio of their standard
205 deviations [*Taylor*, 2001].

206 All datasets are converted to a common 2.5°×2.5° longitude-latitude grid using an
207 interpolation scheme present in Climate Data Operators (CDO) software.

208 The Mann-Kendall test for a trend and Sen's slope estimates were used to detect and quantify
209 trends in annual and seasonal precipitation [*Sen*, 1968]. A trend is considered to be statistically
210 significant at $p<0.05$.

211

212 **3. Results**

213 **3.1 Annual precipitation climatology and trends: A comparison of multiple**
214 **datasets**

215 The spatial pattern of mean annual precipitation derived from high resolution gridded
216 observations (Figure 1a – top left) is broadly similar to studies based on individual stations [*You et*
217 *al.*, 2012]: mean annual precipitation decreases gradually from southeast to northwest. The TP can
218 be divided into northwestern (NW) and southeastern (SE) areas using the isohyet of 400 mm

219 which represents the boundary between semi-arid and semi-humid regions. The dry NW TP is
220 dominated by the westerlies for almost the whole year whereas monsoon precipitation-producing
221 weather systems increase annual precipitation to over 1200 mm in the SE region (Figure 1a).

222 In most cases, the spatial patterns of mean annual precipitation derived from the multi-
223 datasets (Figure 2) are quite similar to the gridded-observations, increasing gradually from NW to
224 SE. However, the more subtle patterns are sometimes different. Some datasets (e.g. ERA-40 and
225 GPCP), show the highest precipitation in the south-west of the region (as opposed to the south-
226 east) and longitudinal contrasts in precipitation are less consistent between datasets than latitudinal
227 ones. Most multi-datasets, with the exception of CMAP2 and MERRA, tend to overestimate mean
228 annual values, particularly in the south of the region.

229 Spatial trends during 1979-2001 for all the multi-datasets are compared in Figure 3. Patterns
230 show more small-scale spatial variance than the mean precipitation field. For the observations
231 (refer back to Figure 1b, top right panel) increasing trends occur in parts of the south and east
232 with weak drying over northern regions. This pattern is most closely replicated by CMAP1 and
233 CMAP2 but NCEP2 and CFSR also show similarities. Other datasets show widely divergent
234 trend maps. NCEP1 and MERRA have widespread negative trends which do not fit in with the
235 observations. ERA-Interim and ERA-40 show lots of local scale variance in trends, with areas of
236 drying and wetting in close proximity.

237 These differences are summarized in Figure 4 for the two sub-regions of the plateau
238 identified earlier (NW and SE). The mean annual precipitation in the NW and SE from
239 observations is 324.3 mm and 751.2 mm, respectively (Figure 4 and also Figures 1c and 1d), with
240 the largest contribution in summer. Mean figures for the NW region for other datasets range from

312.9 mm (MERRA) to 1049.5 mm (20century) but in most cases figures are over-estimates. The same is true in the SE region where ERA-Interim estimates a mean precipitation of nearly 2000 mm. The contrasts in overestimation between datasets are broadly consistent in both regions. CMAP1, CMAP2 and MERRA appear closest to the observations. Trends from observations for the NW and SE TP are +3.99 mm/decade and +16.84 mm/decade, respectively (Figure 4c and d), broadly consistent with previous studies [*Z X Xu et al.*, 2008; *You et al.*, 2012]. Trends in precipitation from NCEP1 and MERRA in particular are strongly negative, and fail to match the wetting shown in the observations. However ERA-Interim, ERA-40 and CFSR show the reverse problem of over-prediction of wetting trends, particularly in the SE. The widely divergent trends in precipitation between datasets are not to be ignored and require further investigation.

3.2 Seasonal patterns

Precipitation in different seasons is dominated by different climate systems, and examination of each season separately may help explain some of the seasonal and regional differences shown in the previous section. The mean seasonal totals for the NW and SE regions for observations (Figure 1e) and each of the nine datasets (Figure 5) are shown. Meanwhile, similar information expressed as a percentage of the annual total is presented in Figure 1f and Figure 6. In the NW TP, most observed precipitation occurs in summer (212.4 mm, accounting for 65.4% of the total annual precipitation) (Figures 1e and 1f), associated with the summer monsoon. Spring, autumn and winter are much drier at 42.5mm (13.1%), 59.9mm (18.5%) and 9.6 mm (3%), respectively (Figure 1f). Similar to the observations, summer precipitation in all the multi-datasets contributes largely to the mean annual total. The summer percentage is highest in the drier NW, but still high in the humid SE.

263 The spatial patterns of mean seasonal precipitation are quite similar to the annual maps. In
264 nearly all seasons most precipitation occurs in the SE part of the plateau. Although summer totals
265 are much higher in the SE region than further NW, the percentage of precipitation which falls in
266 summer in comparison with other seasons (Figure 6) is broadly similar to the NW region. Thus,
267 although absolute amounts differ, there is relatively little difference between datasets in seasonal
268 percentages, suggesting that all of them do simulate monsoonal moisture as the main precipitation
269 source.

270 Figure 7 shows trends in mean seasonal precipitation for each dataset. Trend magnitudes are
271 larger in the SE than the NW but this is partly an artifact of higher seasonal amounts. The
272 observations do not show pronounced seasonality in trends (weak wetting in all seasons). Some
273 datasets on the other hand show pronounced drying in spring (NCEP1) or summer (MERRA),
274 while ERA-40 shows strong wetting in summer. Trends in winter are usually small in all datasets.
275 Thus the inconsistencies which exist between multi-datasets for trend analysis are probably driven
276 by differences in the simulation of monsoonal moisture.

277 **3.3 Taylor diagram analysis**

278 Taylor diagrams provide a concise statistical summary of how well patterns in datasets
279 match each other in terms of their correlation, root-mean-square difference (RMSD) and the ratio
280 of their variances [*Taylor*, 2001]. The Taylor diagrams show the correlation coefficients, standard
281 deviation, and RMSD of precipitation estimates based on a comparison between observations and
282 each multi-dataset in turn. Separate diagrams are shown for annual precipitation in the NW and SE
283 regions (Figure 8) and for each season in the NW (Figure 9) and SE (Figure 10). The radial and
284 angular coordinates represent the magnitude of standard deviation and correlation coefficients

between observed and modeled precipitation respectively. The radial distance from the origin is proportional to the standard deviation between the two patterns. Each multi-dataset is represented by a point on the diagram and the closer point is marked "obs", which is the observations.

On an annual basis, most multi-datasets are closer to the observations in the NW rather than the SE TP. This is particularly marked for GPCP, CMAP1 and CMAP2 (Figure 8 right column). The Taylor figure clearly shows which multi-datasets perform relatively well and have higher correlation coefficients with the observations (e.g. 20century, ERA-Interim, NCEP2 and GPCP in the NW; ERA-Interim and GPCP in the SE). The smallest RMSD is found in GPCP.

The Taylor diagrams on a seasonal basis for the NW region (Figure 9) show the largest RMSD in summer (Figure 9b) and smaller differences in other seasons. GPCP seems closest to observations in the summer. In the SE region (Figure 10) the smallest RMSD in summer again occurs for GPCP. In other seasons differences between datasets are small. The main results represented in Figure 10 are very similar to those on the annual basis, with summer contributing mostly to differences between modeled and observed precipitation.

Much of the difference between multi-data sets and observations has been shown to be in the ways in which they derive temporal trends. The process of removing the effects of a trend (de-trending) allows only short-term fluctuations in precipitation to dominate the variance (Figures 11 and 12). These figures show only the absolute changes in mean annual and seasonal precipitation values respectively, and identify both cyclical patterns and major turning points. These are shown to be similar in most datasets but with enhanced variance in ERA-Interim, particularly in the SE region (Figure 11b and Figure 12 right hand column). Thus inter-annual fluctuations are captured well by most datasets, even if trends are not. The most successful

datasets are different in each region and each season, and there is no one dataset which is obviously the "best". Most multi-datasets can capture the distributions of mean precipitation fairly well but not necessarily trends.

4. Discussion and Conclusions

Spatial and temporal distributions of mean precipitation in the TP during 1979-2001 based on a gridded-observation dataset with high resolution (0.25°×0.25°) have been examined [*Wu and Gao*, 2013; *Xu et al.*, 2009]. Mean annual precipitation increases from NW to SE, and seasonal patterns are broadly similar in both regions. Most precipitation falls in summer [*You et al.*, 2012]. Trends estimated by the Mann-Kendall test [*Sen*, 1968] show that precipitation in all seasons in both NW and SE regions has been increasing with a rate of 3.99 mm/decade in the NW and 16.84 mm/decade in the SE, respectively.

Comparison of precipitation between observations and numerous multi-datasets (reanalyses: NCEP1, NCEP2, ERA-Interim, ERA-40, 20century, MERRA and CFSR, merged analyses: CMAP1, CMAP2 and GPCP) has been performed in the TP during 1979-2001. These multi-datasets capture the broad distributions of mean precipitation, but there exist discrepancies for trends.

Most reanalyses (NCEP1, NCEP2, ERA-Interim, ERA-40, 20century, MERRA and CFSR) overestimate precipitation, particularly in the SE region but MERRA is much closer to the observations for mean precipitation. 20century has particularly large discrepancies. Compared with NCEP1, NCEP2 shows slightly better agreement with observations possibly because NCEP2 incorporates new system components such as simple precipitation assimilation over land surfaces

329 for improved soil wetness [*Kanamitsu et al.*, 2002]. This result is consistent with other findings
330 that show that the spatial patterns of NCEP2 are closer to observations than NCEP1 [*Ma et al.*,
331 2009]. Similarly, ERA-Interim is better than ERA-40, due to improvement in aspects such as
332 reduced spin-up and drift of precipitation and some improvements in the simulation of the diurnal
333 cycle [*Betts et al.*, 2009]. It is also noted that ERA-40 produces reasonable comparisons over the
334 Northern Hemisphere continent, but weak comparisons in the tropical oceans [*Bosilovich et al.*,
335 2008].

336 In recent years, several efforts have been made to improve reanalyses, such as
337 implementing a four-dimensional data assimilation system (e.g. ERA-Interim), utilizing ensemble
338 data assimilation and extending temporal resolution (e.g. 20century) and increasing the horizontal
339 and vertical resolution (e.g. MERRA and CFSR) [*Zhang et al.*, 2013]. These efforts have
340 improved precipitation modelling to some extent, but the precipitation from reanalyses is still to
341 be treated with caution due to the complexity of the processes involved in data assimilation.
342 Figure 13 shows the topography assimilated by NCEP1, NCEP2, ERA-40 and ERA-Interim.
343 Because the TP is a region with sharp elevation bands and complex topography, the representation
344 of surface terrain in the reanalysis systems is still different in different reanalyses. This could
345 account for some of the discrepancies between them. In particular moisture convergence is
346 sensitive to small scale terrain. This is shown by differences in mean annual water vapor (vector,
347 unit is kg/(s·hPa·m)) and moisture divergence (shaded, unit is 10^{-7} kg/(s·hPa·m^2)) at 500 hPa
348 during 1979-2001 among NCEP1, NCEP2, ERA-40 and ERA-Interim (Figure 14).

349 Most of the merged analysis datasets (CMAP1, CMAP2 and GPCP) also overestimate
350 precipitation in both regions on an annual and seasonal basis, but biases are smaller than the

351 reanalyses. Overestimations appear worst in regions with complex topography. CMAP2 has the
352 smallest biases, indicating the best choice for precipitation assessment.

353 Taylor diagrams are used to compare skill in precipitation modelling between multi-
354 datasets. The diagrams can clearly indicate which datasets are nearest to observations. Relatively
355 low RMSD are found in CMAP2 and GPCP, suggesting that they may be used as the reference
356 standard.

357 Compared with the reanalyses (NCEP1, NCEP2, ERA-Interim, ERA-40, 20century, MERRA
358 and CFSR), CMAP1, CMAP2 and GPCP show more similar trend magnitudes to the observations
359 as well as more similar mean distributions. Thus merged analysis precipitation appears more
360 reliable than reanalyses, consistent with other studies in China [*Ma et al.*, 2009; *Zhao and Fu*,
361 2006]. Over the whole of China, precipitation products from multi-datasets and observational
362 stations have been compared [*Ma et al.*, 2009; *Zhao and Fu*, 2006]. This indicated that CMAP1,
363 CMAP2 and GPCP agreed more closely with the observations than reanalysis data (NCEP1,
364 NCEP2 and ERA40), and that ERA40 was more reliable than NCEP [*Ma et al.*, 2009].

365 Reanalysis datasets are the output of data assimilation combined with available observations
366 and a background model forecast. Thus uncertainties emerge, related to the model physical
367 parameterizations [*Betts et al.*, 2006; *Bosilovich et al.*, 2008]. In addition, the topography can
368 influence the bias between observations and multi-datasets due to the difference between
369 assimilated and actual topography. In China, *Ma et al.*, [2009] suggested that the reanalyses
370 overestimation of precipitation was a more serious issue in regions with complex terrain and less
371 of a problem in flatter regions. Models may not resolve precipitation in areas of complex
372 topographic relief, especially in the regions with drastic elevation changes where moisture

convergence is often locally determined, and local convective precipitation is strongly dependent upon local thermal forcing of the terrain.

Although the merged datasets in this study are closer to the observations than the reanalyses, contrasting retrieval algorithms, input data, treatment of gauge uncertainties, and quality flags can also result in differences with observations [*Adler et al.*, 2003; *Bosilovich et al.*, 2008; *Huffman et al.*, 2009; *Huffman et al.*, 1997; *Xie and Arkin*, 1997; *Yin et al.*, 2004]. For example, *Yin et al.,* [2004] found that GPCP and CMAP (CMAP1 and CMAP2) have less/more in common over ocean/land areas, while different merging algorithms can produce a substantial discrepancy in sensitive areas such as equatorial West Africa. GPCP and CMAP exhibited good agreement over the Southern Hemisphere, and also over land in the Northern Hemisphere. In the tropical ocean however, CMAP was wetter than GPCP, and this effect reversed over high latitude oceans [*Yin et al.*, 2004]. GPCP is planned to feature a finer time and space resolution in the near future [*Huffman et al.*, 2009], suggesting that this product is updated continually and that it should be taken as a good reference for studying precipitation over the TP. Clearly the discrepancies between different datasets mean that continuing attention should be paid to the selection of datasets for representing precipitation in the TP region and its trends.

Acknowledgments. This study is supported by the State Key Program of National Natural Science Foundation of China (41230528), National Natural Science Foundation (41201072); Jiangsu Specially-Appointed Professor (R2013T07), Jiangsu Natural Science Funds for Distinguished Young Scholar "BK20140047", and the Priority Academic Program Development

394 of Jiangsu Higher Education Institutions (PAPD). We are very grateful to the reviewers for their
395 constructive comments and thoughtful suggestions.

396

397 Reference

398 Adler, R. F., et al. (2003), The version-2 global precipitation climatology project (GPCP) monthly
399 precipitation analysis (1979-present), *Journal of Hydrometeorology*, *4*(6), 1147-1167.

400 Allan, R. P., and B. J. Soden (2008), Atmospheric warming and the amplification of precipitation
401 extremes, *Science*, *321*(5895), 1481-1484.

402 Betts, A. K., M. Kohler, and Y. C. Zhang (2009), Comparison of river basin hydrometeorology in
403 ERA-Interim and ERA-40 reanalyses with observations, *Journal of Geophysical Research-*
404 *Atmospheres*, *114*, D02101.

405 Betts, A. K., M. Zhao, P. A. Dirmeyer, and A. C. M. Beljaars (2006), Comparison of ERA40 and
406 NCEP/DOE near-surface data sets with other ISLSCP-II data sets, *Journal of Geophysical*
407 *Research-Atmospheres*, *111*, D22S04.

408 Bosilovich, M. G., J. Chen, F. R. Robertson, and R. F. Adler (2008), Evaluation of global
409 precipitation in reanalyses, *Journal of Applied Meteorology and Climatology*, *47*(9), 2279-2299.

410 Compo, G. P., et al. (2011), The Twentieth Century Reanalysis Project, *Q. J. R. Meteorol. Soc.*,
411 *137*(654), 1-28.

412 Dee, D. P., et al. (2011), The ERA-Interim reanalysis: configuration and performance of the data
413 assimilation system, *Q. J. R. Meteorol. Soc.*, *137*(656), 553-597.

414 Duan, A. M., and G. X. Wu (2005), Role of the Tibetan Plateau thermal forcing in the summer
415 climate patterns over subtropical Asia, *Climate Dynamics*, *24*(7-8), 793-807.

Duan, A. M., G. Wu, Y. Liu, Y. Ma, and P. Zhao (2012), Weather and climate effects of the Tibetan Plateau, *Advances in Atmospheric Sciences*, *29*(5), 978-992.

Feng, L., and T. J. Zhou (2012), Water vapor transport for summer precipitation over the Tibetan Plateau: Multidata set analysis, *Journal of Geophysical Research-Atmospheres*, *117*, D20114.

Huffman, G. J., R. F. Adler, D. T. Bolvin, and G. Gu (2009), Improving the global precipitation record: GPCP Version 2.1, *Geophysical Research Letters*, *36*, L17808.

Huffman, G. J., R. F. Adler, P. Arkin, A. Chang, R. Ferraro, A. Gruber, J. Janowiak, A. McNab, B. Rudolf, and U. Schneider (1997), The Global Precipitation Climatology Project (GPCP) Combined Precipitation Dataset, *Bulletin of the American Meteorological Society*, *78*(1), 5-20.

Immerzeel, W. W., L. P. H. van Beek, and M. F. P. Bierkens (2010), Climate Change Will Affect the Asian Water Towers, *Science*, *328*(5984), 1382-1385.

IPCC (2007), Summary for Policymakers of Climate change 2007: The Physical Science Basis. Contribution of Working Group I to the Fourth Assessment Report of the Intergovernmental Panel on Climate Change *Cambridge, UK: Cambridge University Press*.

IPCC (2013), Summary for Policymakers of Climate change 2013: The Physical Science Basis. Contribution of Working Group I to the Fifth Assessment Report of the Intergovernmental Panel on Climate Change *Cambridge, UK: Cambridge University Press*.

Joshi, M. K., and A. C. Pandey (2011), Trend and spectral analysis of rainfall over India, *Journal of Geophysical Research-Atmospheres*, *116*, D06104.

Kalnay, E., et al. (1996), The NCEP/NCAR 40-year reanalysis project, *Bulletin of the American Meteorological Society*, *77*(3), 437-471.

Kanamitsu, M., W. Ebisuzaki, J. Woollen, S. K. Yang, J. J. Hnilo, M. Fiorino, and G. L. Potter (2002), NCEP-DOE AMIP-II reanalysis (R-2), *Bulletin of the American Meteorological Society*, *83*(11), 1631-1643.

Kang, S. C., Y. W. Xu, Q. L. You, W. A. Flugel, N. Pepin, and T. D. Yao (2010), Review of climate and cryospheric change in the Tibetan Plateau, *Environ. Res. Lett.*, *5*(1), 015101.

Kistler, R., et al. (2001), The NCEP-NCAR 50-year reanalysis: Monthly means CD-ROM and documentation, *Bulletin of the American Meteorological Society*, *82*(2), 247-267.

Liu, X. D., and Z. Y. Yin (2001), Spatial and temporal variation of summer precipitation over the eastern Tibetan Plateau and the North Atlantic oscillation, *J. Clim.*, *14*(13), 2896-2909.

Ma, L. J., T. Zhang, O. W. Frauenfeld, B. S. Ye, D. Q. Yang, and D. H. Qin (2009), Evaluation of precipitation from the ERA-40, NCEP-1, and NCEP-2 Reanalyses and CMAP-1, CMAP-2, and GPCP-2 with ground-based measurements in China, *Journal of Geophysical Research-Atmospheres*, *114*, D09105.

New, M., D. Lister, M. Hulme, and I. Makin (2002), A high-resolution data set of surface climate over global land areas, *Climate Research*, *21*, 1-25.

Ohmura, A., and M. Wild (2002), Is the hydrological cycle accelerating?, *Science*, *298*(5597), 1345-1346.

Qiu, J. (2008), The third pole, *Nature*, *454*(7203), 393-396.

Rienecker, M. M., et al. (2011), MERRA: NASA's Modern-Era Retrospective Analysis for Research and Applications, *J. Clim.*, *24*(14), 3624-3648.

Saha, S., et al. (2010), The NCEP Climate Forecast System Reanalysis, *Bulletin of the American Meteorological Society*, *91*(8), 1015-1057.

Sen, P. K. (1968), Estimates of regression coefficient based on Kendall's tau, *Journal of the American Statistical Association*, *63*, 1379-1389.

Serreze, M. C., and C. M. Hurst (2000), Representation of mean Arctic precipitation from NCEP-NCAR and ERA reanalyses, *J. Clim.*, *13*(1), 182-201.

Taylor, K. E. (2001), Summarizing multiple aspects of model performance in a single diagram, *Journal of Geophysical Research-Atmospheres*, *106*(D7), 7183-7192.

Trenberth, K. E. (2011), Changes in precipitation with climate change, *Climate Research*, *47*(1-2), 123-138.

Trenberth, K. E., and C. J. Guillemot (1998), Evaluation of the atmospheric moisture and hydrological cycle in the NCEP/NCAR reanalyses, *Climate Dynamics*, *14*(3), 213-231.

Uppala, S. M., et al. (2005), The ERA-40 re-analysis, *Q. J. R. Meteorol. Soc.*, *131*(612), 2961-3012.

Wu, J., and X. J. Gao (2013), A gridded daily observation dataset over China region and comparison with the other datasets, *Chinese Journal of Geophysics*, *56*(4), 1102-1111.

Xie, P. P., and P. A. Arkin (1997), Global precipitation: A 17-year monthly analysis based on gauge observations, satellite estimates, and numerical model outputs, *Bulletin of the American Meteorological Society*, *78*(11), 2539-2558.

Xu, X. D., C. G. Lu, X. H. Shi, and S. T. Gao (2008), World water tower: An atmospheric perspective, *Geophysical Research Letters*, *35*(20), L20815.

Xu, Y., X. J. Gao, S. Y. Yan, C. H. Xu, Y. Shi, and F. Giorgi (2009), A daily temperature dataset over China and its application in validating a RCM simulation, *Advances in Atmospheric Sciences*, *26*(4), 763-772.

481 Xu, Z. X., T. L. Gong, and J. Y. Li (2008), Decadal trend of climate in the Tibetan Plateau -
482 regional temperature and precipitation, *Hydrological Processes*, *22*(16), 3056-3065.
483 Yang, K., B. S. Ye, D. G. Zhou, B. Y. Wu, T. Foken, J. Qin, and Z. Y. Zhou (2011), Response of
484 hydrological cycle to recent climate changes in the Tibetan Plateau, *Climatic Change*, *109*(3-4),
485 517-534.
486 Yeh, T. C., and Y. X. Gao (1979), Meteorology of the Qinghai-Xizang (Tibet) Plateau (in
487 Chinese), *Science Press, Beijing.*
488 Yin, X. G., A. Gruber, and P. Arkin (2004), Comparison of the GPCP and CMAP merged gauge-
489 satellite monthly precipitation products for the period 1979-2001, *Journal of Hydrometeorology*,
490 *5*(6), 1207-1222.
491 You, Q. L., K. Fraedrich, G. Y. Ren, B. S. Ye, X. H. Meng, and S. C. Kang (2012),
492 Inconsistencies of precipitation in the eastern and central Tibetan Plateau between surface adjusted
493 data and reanalysis, *Theoretical and Applied Climatology*, *109*, 485-496.
494 Zhang, Q., H. Kornich, and K. Holmgren (2013), How well do reanalyses represent the southern
495 African precipitation?, *Climate Dynamics*, *40*, 951-962.
496 Zhao, T., and C. Fu (2006), Comparison of products from ERA-40, NCEP-2, and CRU with
497 station data for summer precipitation over China, *Advances in Atmospheric Sciences*, *23*(4), 593-
498 604.
499
500
501
502

Table

Table 1. Summary of the observations and multi-datasets in this study

Name	Organization	Temporal resolution	Horizontal resolution	Sources	References
NCEP1	NCEP/NCAR	1948-present	2.5°×2.5°	http://www.esrl.noaa.gov	[*Kalnay et al.*, 1996]
NCEP2	NCEP/DOE	1979-present	2.5°×2.5°	http://www.esrl.noaa.gov	[*Kanamitsu et al.*, 2002]
CMAP1	NOAA	1979-2009	2.5°×2.5°	http://www.cpc.ncep.noaa.gov	[*Xie and Arkin*, 1997]
CMAP2	NOAA	1979-2009	2.5°×2.5°	http://www.cpc.ncep.noaa.gov	[*Xie and Arkin*, 1997]
ERA-Interim	ECMWF	1979-present	1.5°×1.5°	http://www.ecmwf.int	[*Dee et al.*, 2011]
ERA-40	ECMWF	1957-2002.08	2.5°×2.5°	http://www.ecmwf.int	[*Uppala et al.*, 2005]
GPCP	NASA	1979-2009	2.5°×2.5°	http://precip.gsfc.nasa.gov	[*Adler et al.*, 2003]
20Century	NOAA/ESRL PSD	1871-2011	2.5°×2.5°	http://www.esrl.noaa.gov	[*Compo et al.*, 2011]
MERRA	NASA GMAO	1979-present	0.5°×0.5°	http://disc.sci.gsfc.nasa.gov	[*Rienecker et al.*, 2011]
CFSR	NCEP	1979-present	0.5°×0.5°	http://cfs.ncep.noaa.gov	[*Saha et al.*, 2010]
Observation	CMA	1961-2010	0.25°×0.25°	http://www.cma.gov.cn	[*Xu et al.*, 2009]

518 **Figure**

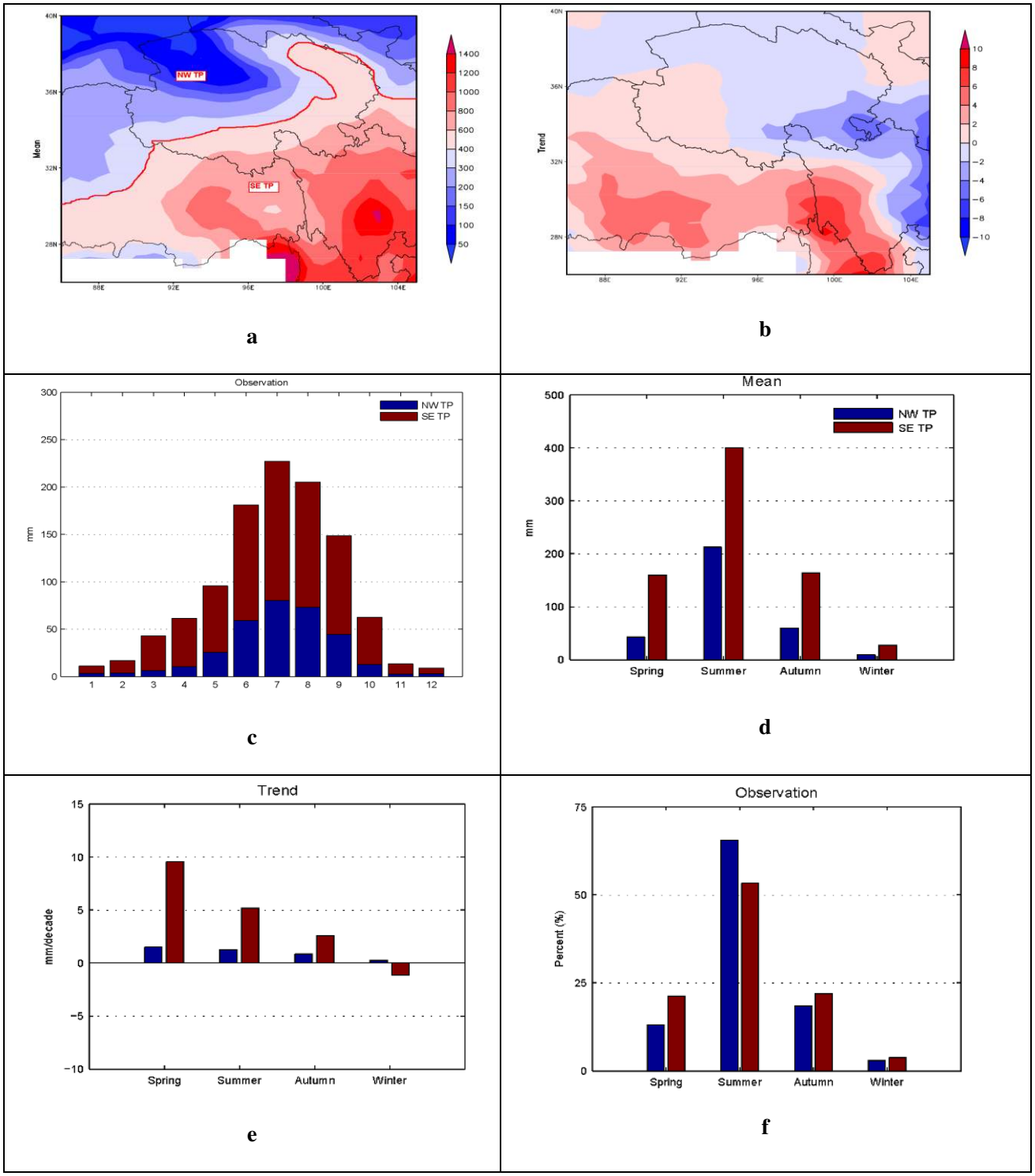

519 **Figure 1.** Characteristics of precipitation in the TP during 1979-2001 from observations: a) annual

520 mean (mm), b) spatial trends (mm/decade), c) regional monthly mean (mm), d) regional seasonal

521 mean (mm), e) regional trends (mm/decade) and f) percent of precipitation in each season(%). The

whole TP is divided into northwestern (NW) and southeastern (SE) regions by the red isohyet of 400 mm, representing the boundary between semi-arid and semi-humid regions.

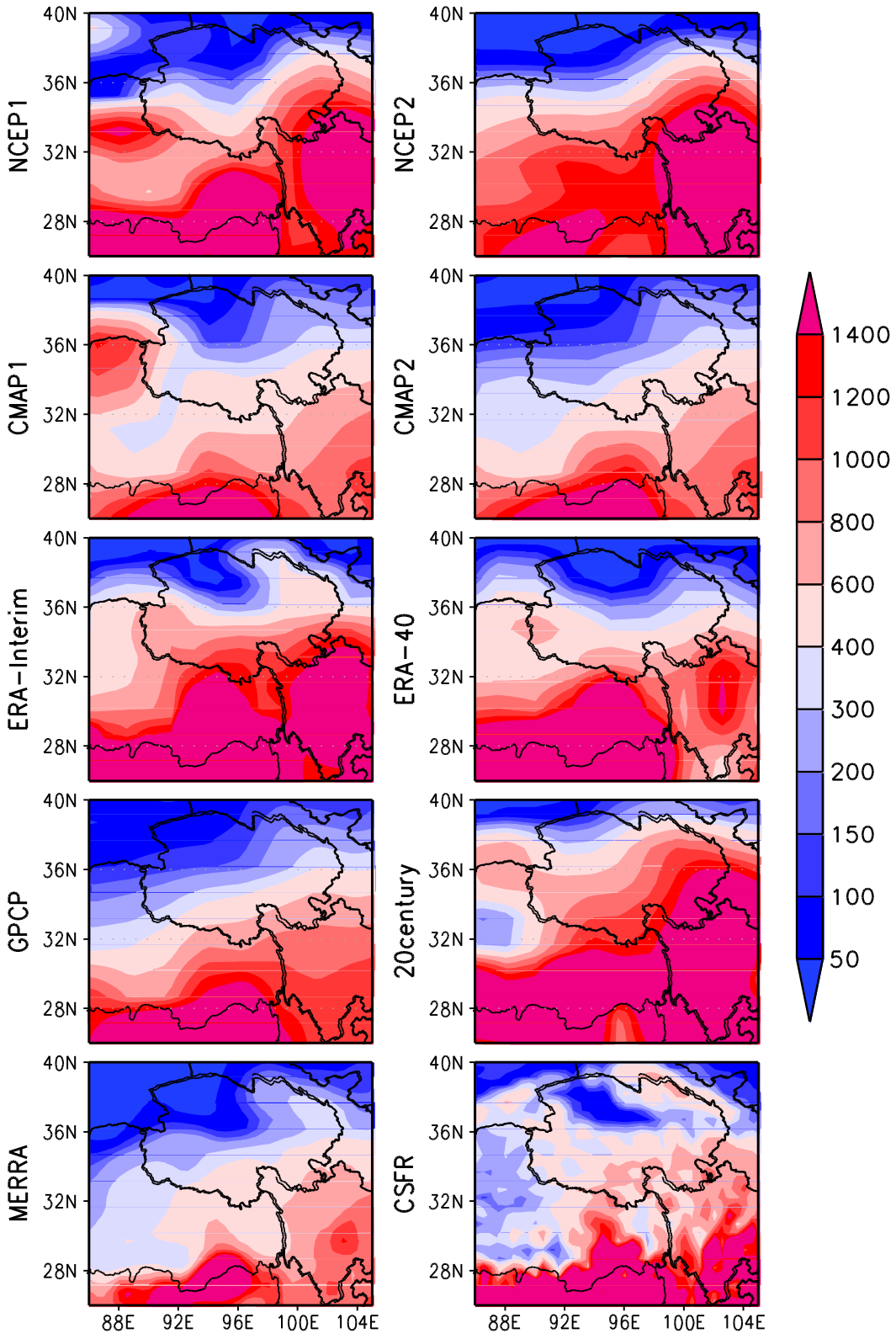

542

543 **Figure 2.** Mean annual precipitation (mm) in the TP during 1979-2001 from various multi-

544 datasets. The multi-datasets include NCEP1, NCEP2, CMAP1, CMAP2, ERA-Interim, ERA-40,

545 GPCP, 20century, MERRA and CFSR, respectively.

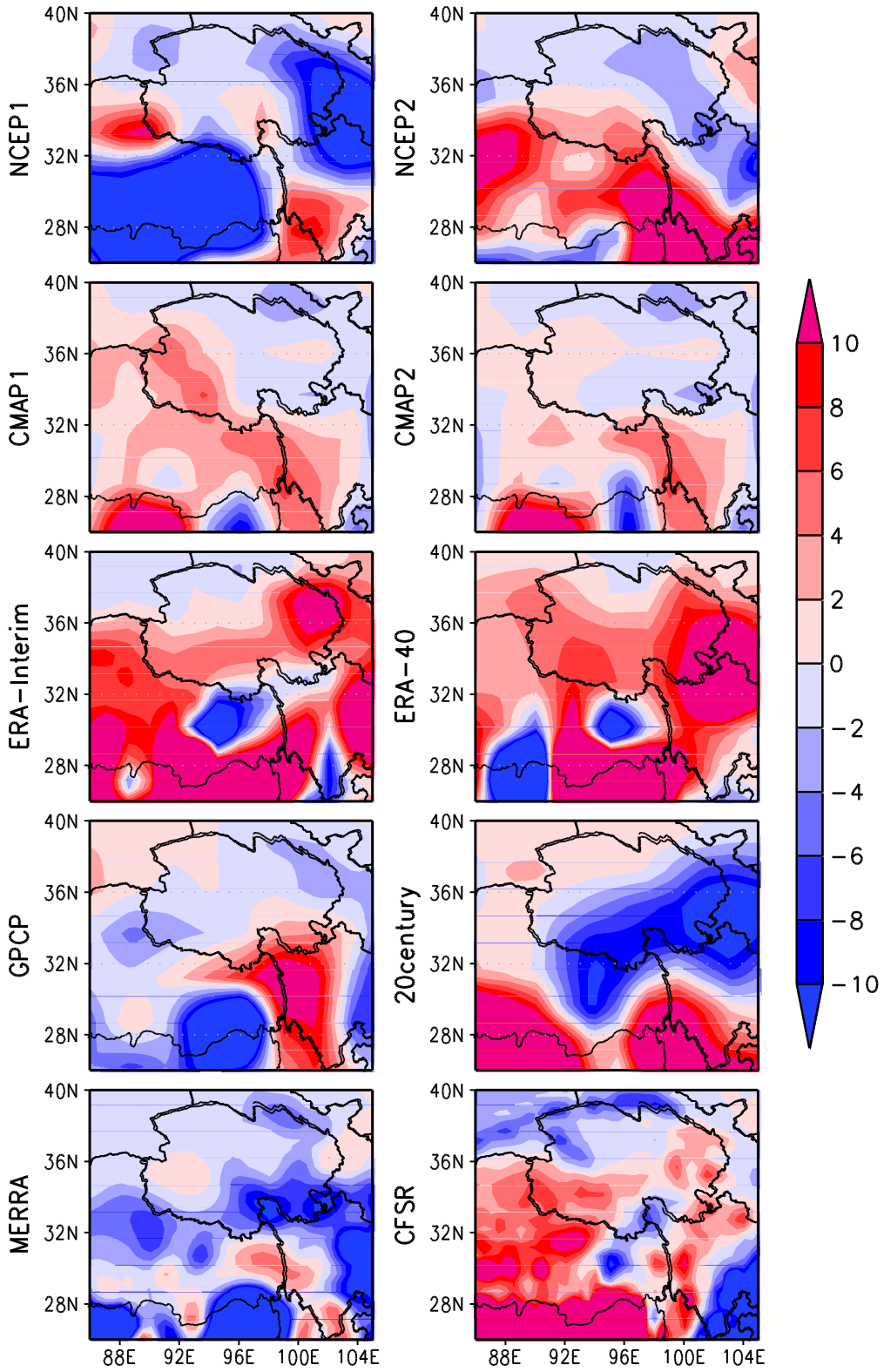

546

547 **Figure 3.** Spatial patterns of trends (mm/decade) of mean annual precipitation in the TP during

548 1979-2001 from various multi-datasets (same as Figure 2). Trends are calculated by the Mann-

549 Kendall test.

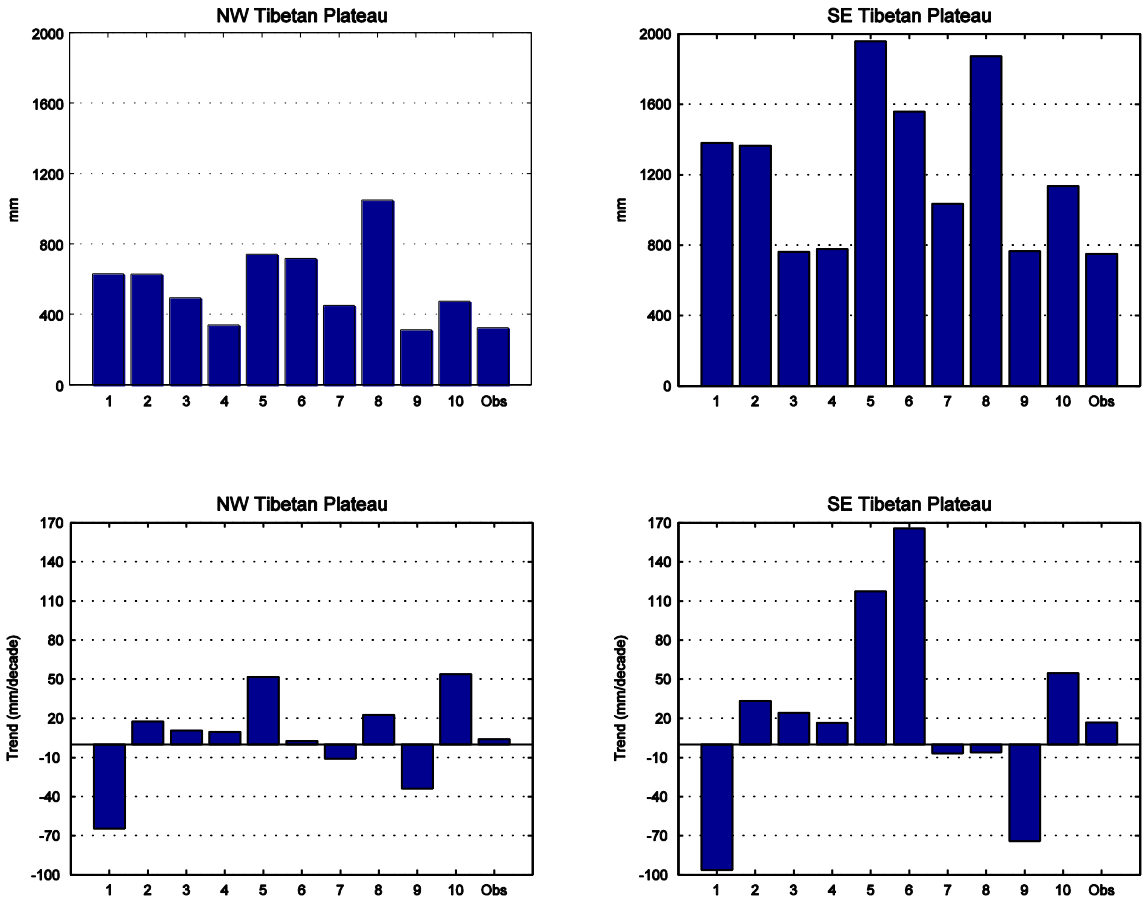

Figure 4. Means and trends of mean annual precipitation in the NW and SE TP during 1979-2001 from observations and multi-datasets. The units for mean precipitation and trends are mm and mm/decade, respectively. The trend is calculated by the Mann-Kendall statistical test. Numbers 1 to 10 represent NCEP1, NCEP2, CMAP1, CMAP2, ERA-Interim, ERA-40, GPCP, 20century, MERRA, CFSR and observations, respectively.

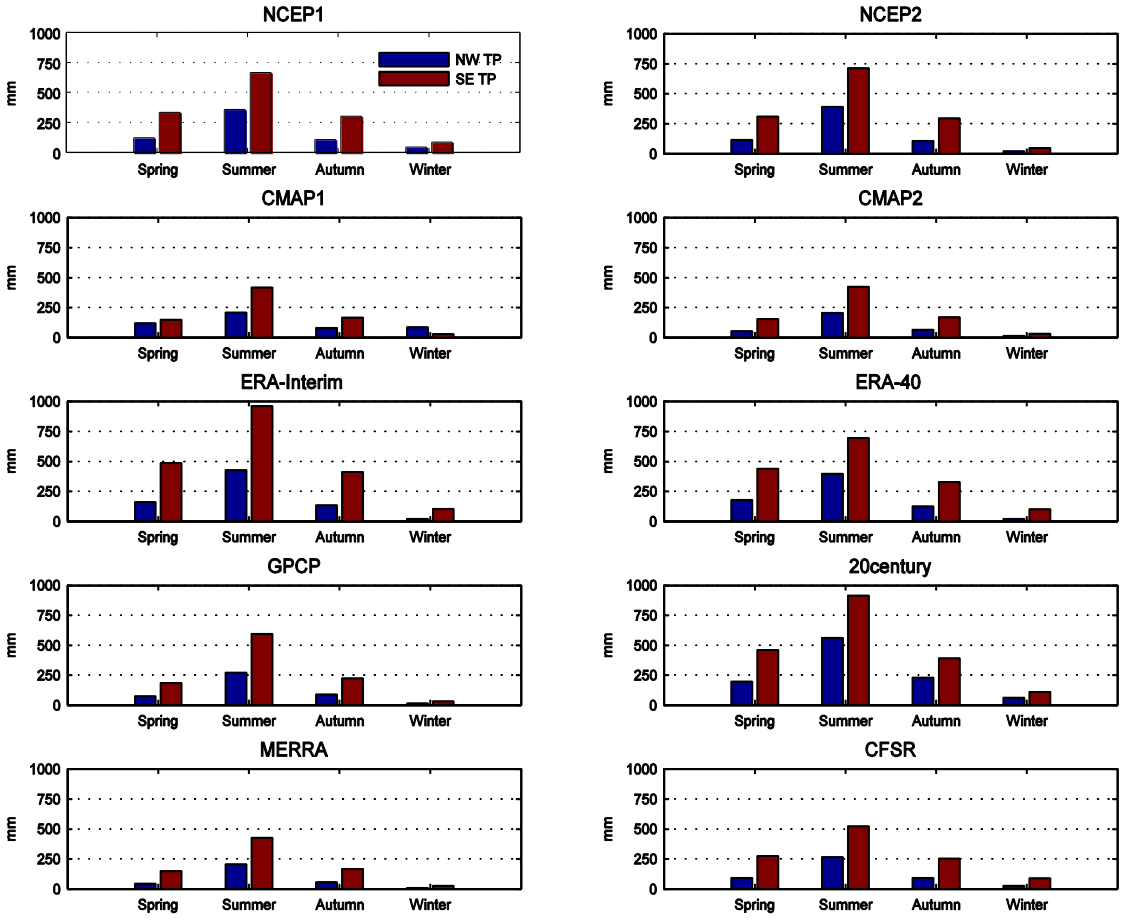

Figure 5. Mean seasonal precipitation in the TP during 1979-2001 from various multi-datasets.

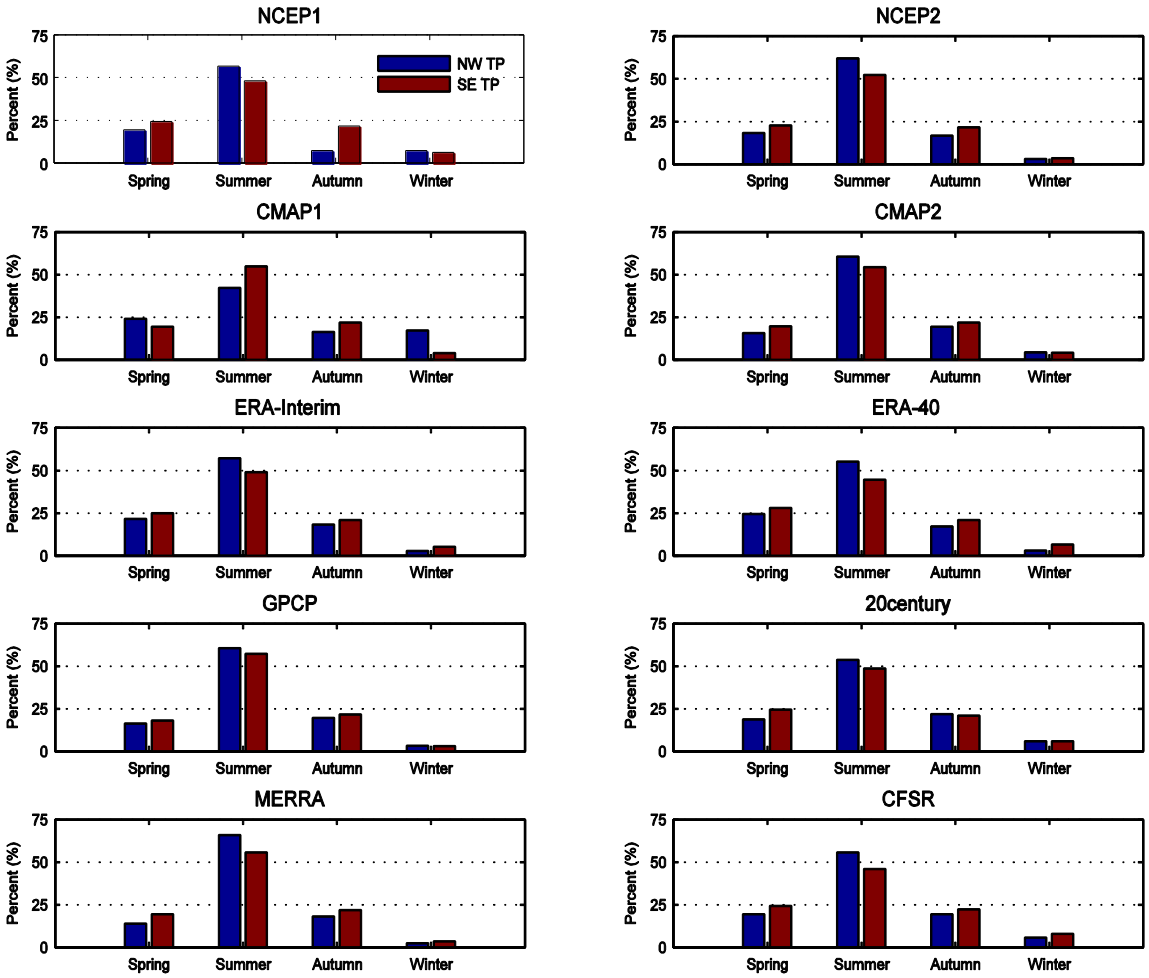

558

559 **Figure 6.** Seasonal precipitation (%: mean seasonal precipitation divided by mean annual

560 precipitation) in the TP during 1979-2001 from various multi-datasets.

561

562

563

564

565

566

567

568

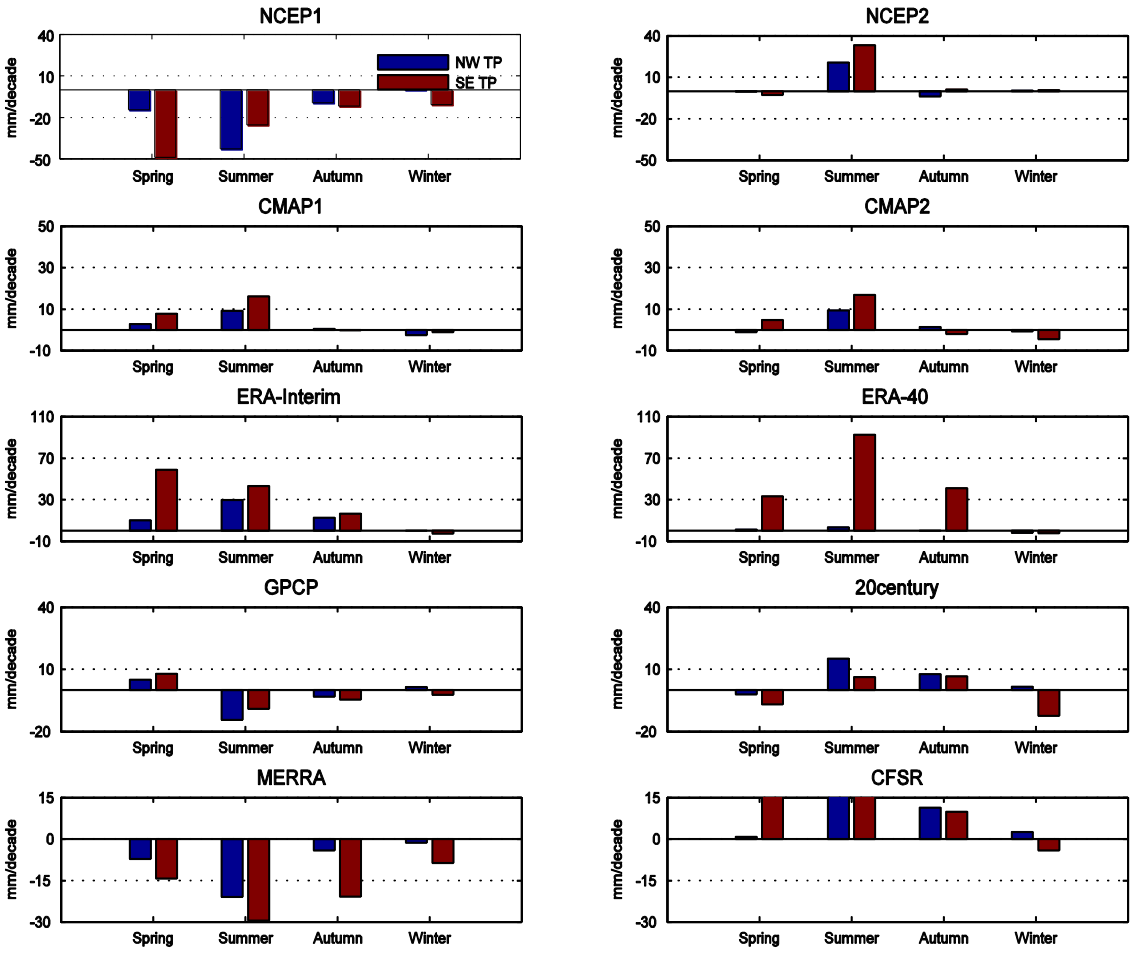

Figure 7. Trends of mean seasonal precipitation in the TP during 1979-2001 from various multi-datasets.

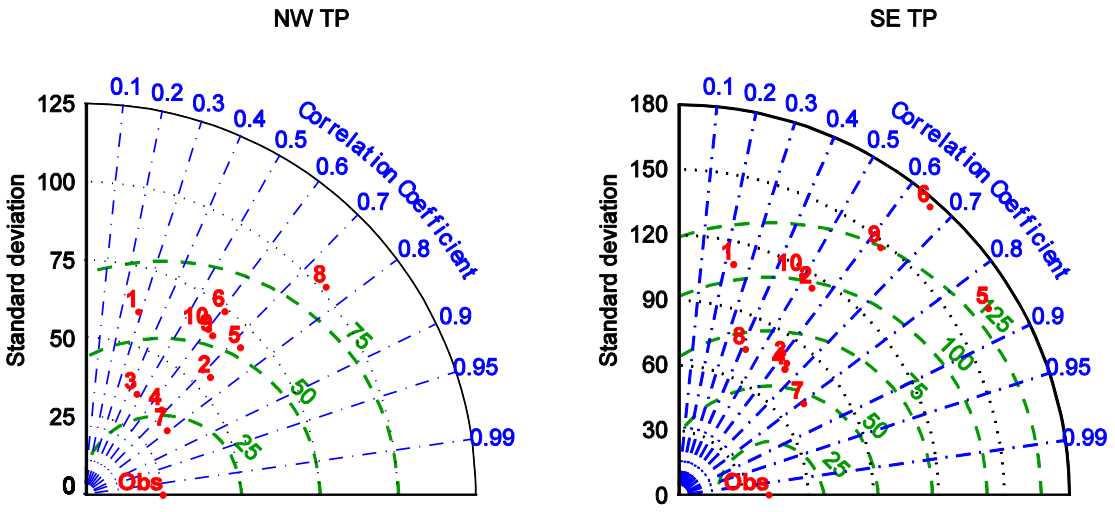

581

582 **Figure 8**. Taylor diagrams showing correlation coefficients, standard deviation, and root-mean-

583 square difference (RMSD) of mean annual precipitation as simulated by observations and various

584 multi-datasets in the NW (left panel) and SE (right panel) TP. Numbers 1 to 10 represent NCEP1,

585 NCEP2, CMAP1, CMAP2, ERA-Interim, ERA-40, GPCP, 20century, MERRA and CFSR,

586 respectively. The radial coordinate (y axis) gives the magnitude of standard deviation, and the

587 concentric semi-circles are the RMSD values. The angular coordinate shows the correlation

588 coefficient.

589

590

591

592

593

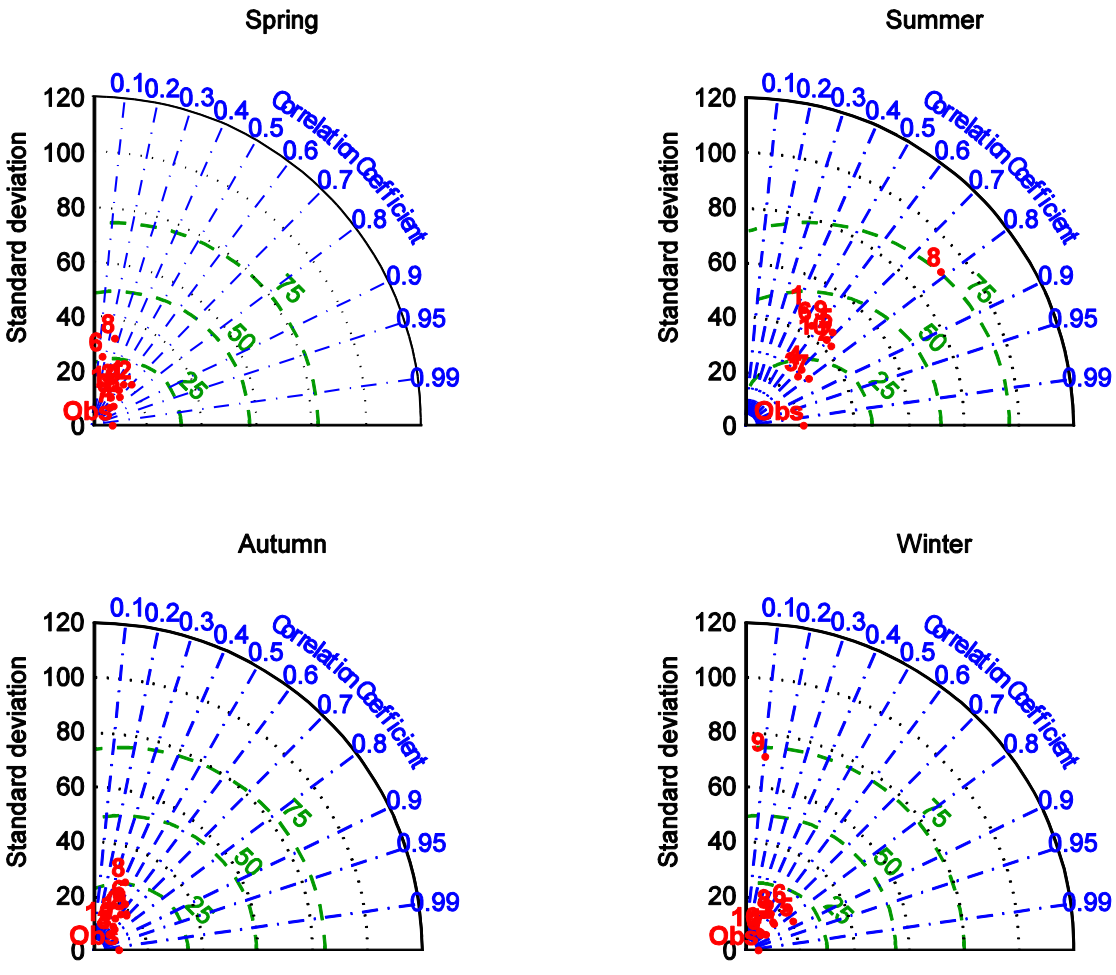

Figure 9. Same as Figure 8 but for the NW TP on a seasonal basis.

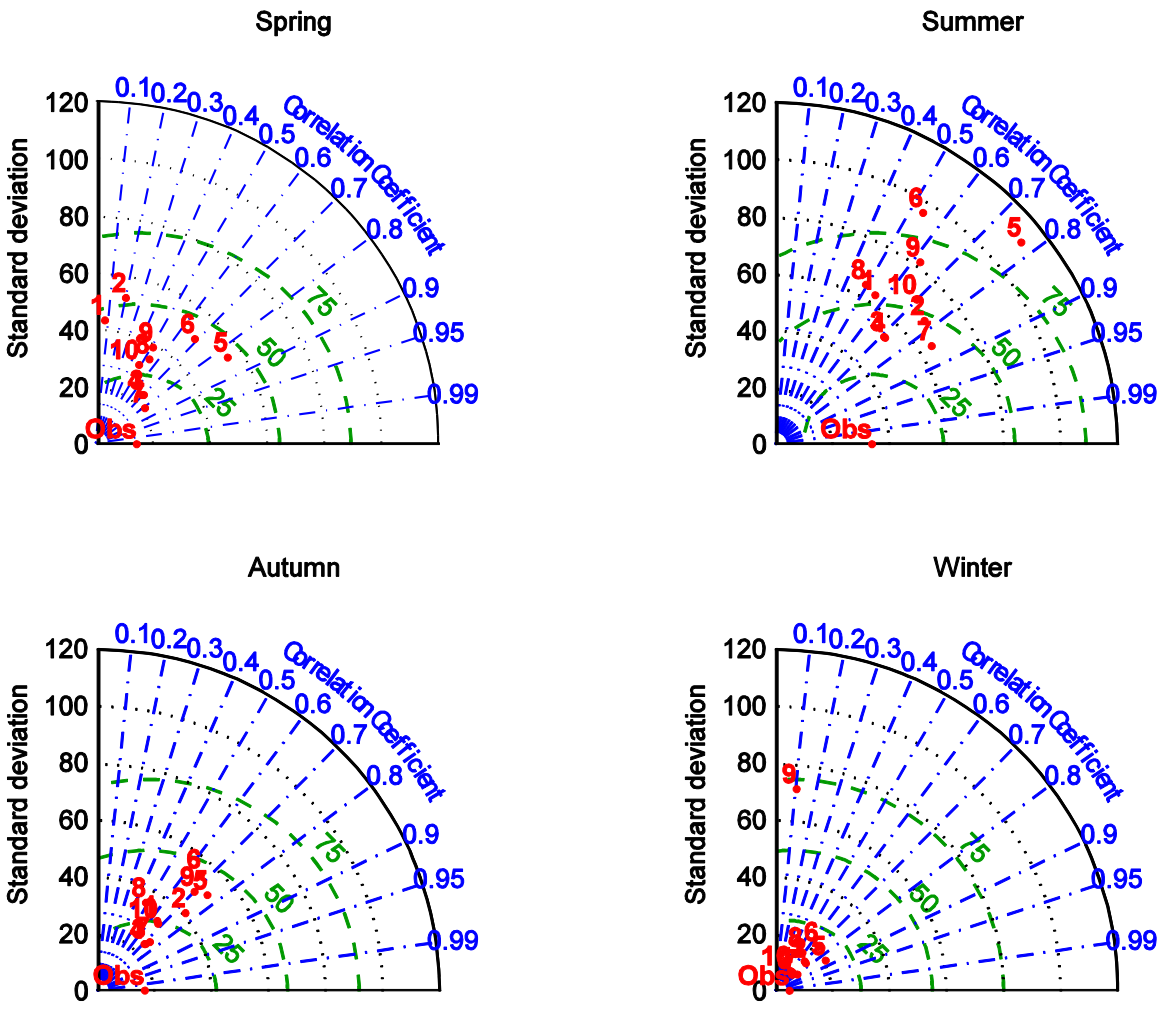

596

597 **Figure 10**. Same as Figure 8 but for the SE TP on a seasonal basis.

598

599

600

601

602

603

604

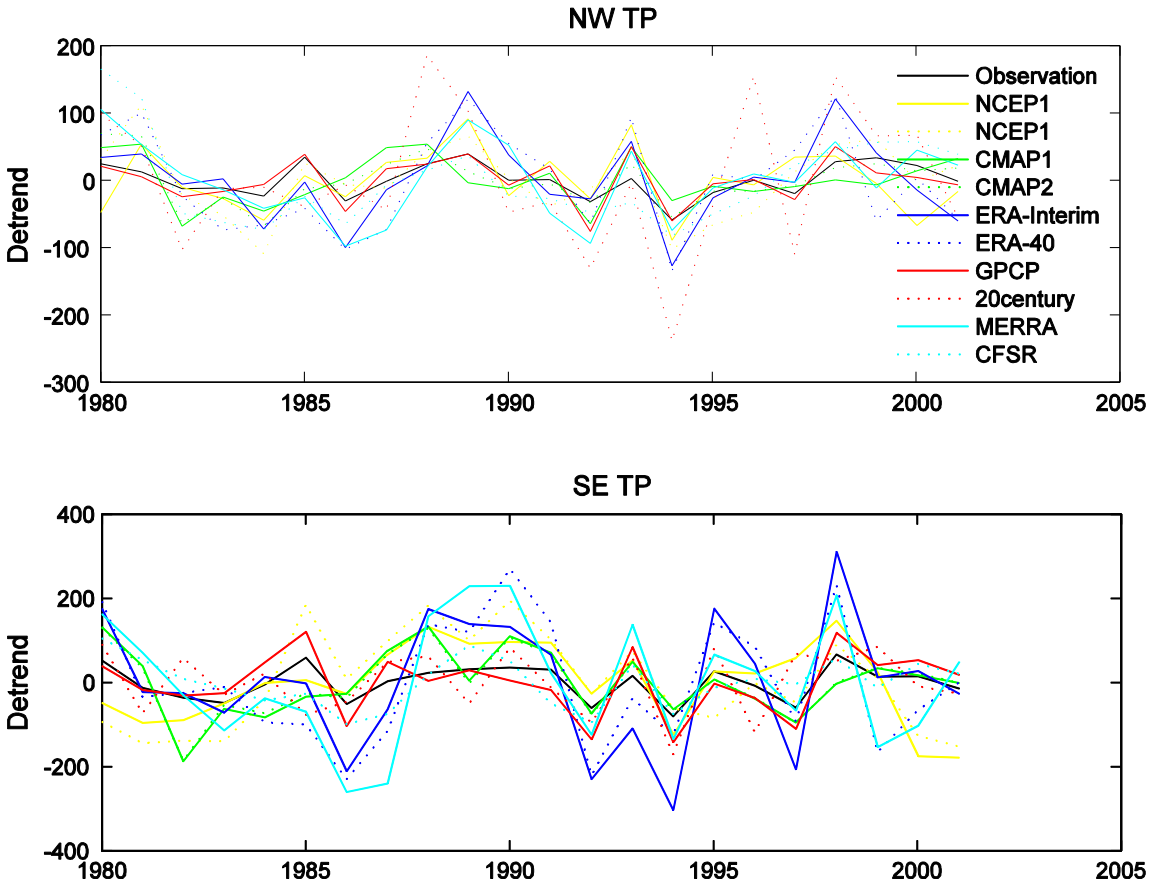

605

606 **Figure 11.** Detrended mean annual precipitation anomaly in the NW (top panel) and SE (bottom

607 panel) TP during 1979-2001 from observations and multi-datasets. The multi-datasets include

608 NCEP1, NCEP2, CMAP1, CMAP2, ERA-Interim, ERA-40, GPCP, 20century, MERRA and

609 CFSR, respectively.

610

611

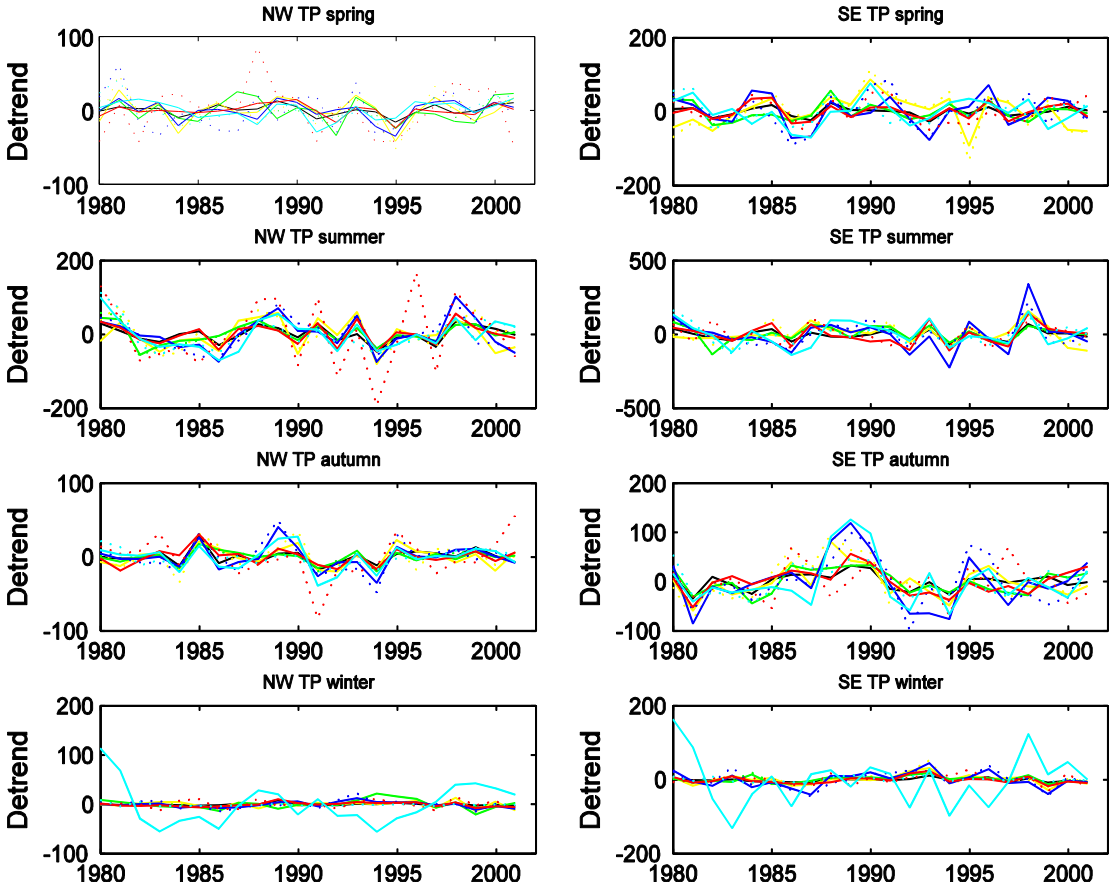

Figure 12. Same as Figure 11 but for mean seasonal precipitation anomaly.

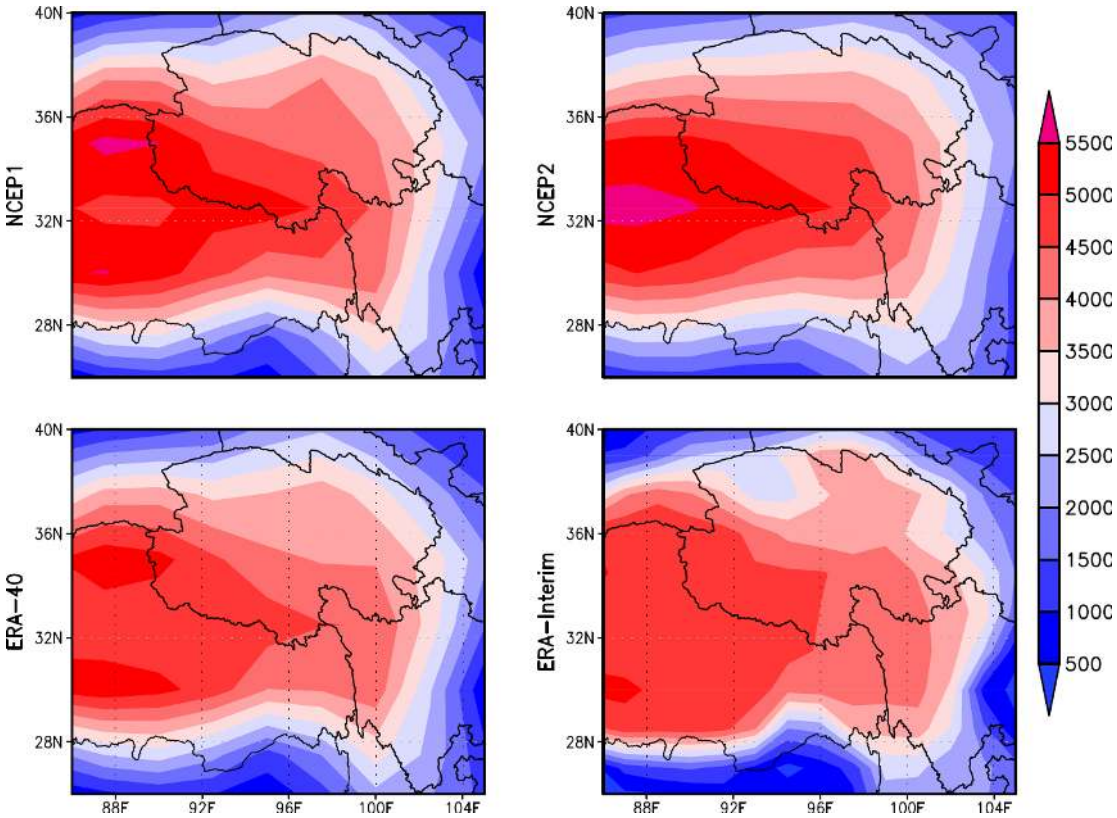

Figure 13. Topography (m) assimilated by NCEP1, NCEP2, ERA-40 and ERA-Interim.

630

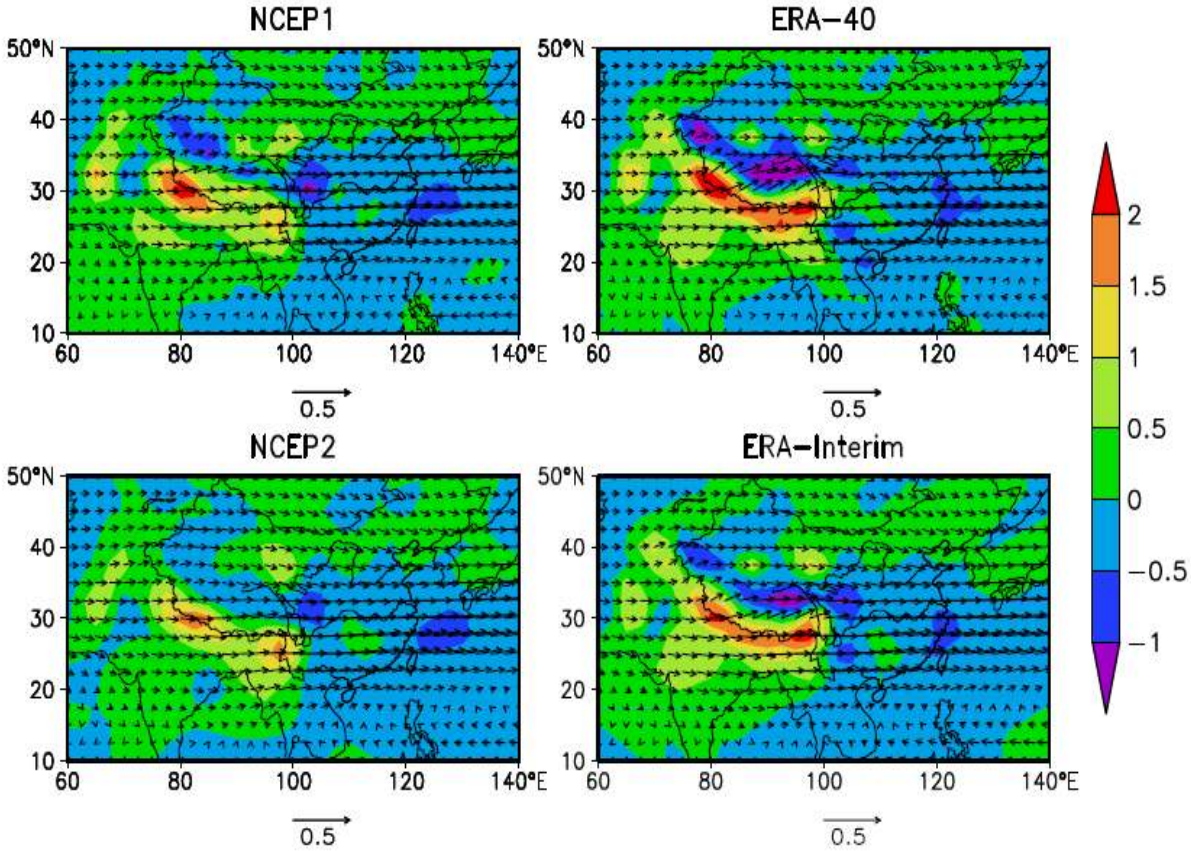

631

632 **Figure 14.** Annual mean water vapor (vector, unit is kg/(s·hPa·m)) and moisture divergence

633 (shaded, unit is 10^{-7} kg/(s·hPa·m^2)) at 500 hPa during 1979-2001 in NCEP1, NCEP2, ERA-40 and

634 ERA-Interim.

635

636

637

638